Deep cerebral lesions, involving basal ganglia, internal capsules, thalamus, were also found in 9 patients ≤7 d of onset. The distributions of deep cerebral lesions (none/unilateral/bilateral) ≤7 d of onset showed significant correlations with neurological prognoses (gross motor functions: $p < 0.01$; developmental or intellectual quotient scores: $p < 0.01$).

Interpretation: Cortical lesions were main findings of DWI in NHSE in the early period. Bilateral deep cerebral lesions ≤7 d were highly indicative of poor motor and cognitive outcomes.

Keywords: Magnetic resonance imaging; Cortical lesions; Diffusion weighted imaging; Herpes simplex encephalitis; Early diagnosis; Neonate

1. Introduction

Neonatal herpes simplex encephalitis (NHSE) is a rapidly progressive, rare infectious disease (mortality rate, approximately 50% in untreated newborns) [1,2]. Although antiviral therapy decreases mortality, 56–70% of survivors experience significant neurological sequelae [1–5]. Early diagnosis is difficult because initial symptoms are usually nonspecific. Herpes simplex virus (HSV) DNA polymerase chain reaction is essential for NHSE diagnosis [1–3]. However, due to the lack of rapidly available diagnostic results (i.e., within hours) and the possibility of false-negative results [6], these viral infections are difficult to correctly diagnose in a timely manner; another method for the early diagnosis of NHSE needs to be established [7].

Magnetic resonance imaging (MRI) of infants with NHSE in acute and subacute stages reveals lesions in the cerebral cortex, white matter, basal ganglia, brainstem, and cerebellum [8–15]. Lesions detected with diffusion-weighted imaging (DWI) show up more clearly than lesions detected with conventional MRI [11,15]. Only 3 cases were reported wherein DWI were demonstrated within 48 h of onset [14,15]. Kubota et al., using DWI, reported a case with progression of lesions from the cerebral cortex to subcortical white matter during 72 h of onset [14]. The correlations between early DWI lesion patterns and time point of the scans have not been reported.

DWI has been applied to predict patient prognosis in neonatal hypoxic ischemic injury [16]. DWI lesions in bilateral posterior limbs of the internal capsule were correlated with poor outcome of motor functions in infants. For NHSE, the correlation between DWI lesion patterns and patient prognosis has not been established.

We analyzed DWI data and the time point of scan. We hypothesize (1) DWI is most sensitive at the early stage, (2) the lesion distribution changes over a period of time, and (3) early DWI findings can correlate with the outcome of motor and cognitive function. We tested these hypotheses by conducting a retrospective, multicenter study of DWI findings in patients with NHSE.

2. Method

2.1. Patients and clinical data

The inclusion criteria were acute symptoms including seizure, lethargy, and feeding impairment, which appeared within 28 d of birth; HSV infection confirmed by virological examinations, including antibody/polymerase chain reaction (PCR) in serum/cerebrospinal fluid or viral culture; and MRI, including DWI, performed within 7 d of onset. The study covered newborns diagnosed with NHSE between September 2001 and August 2011. A questionnaire was sent to 214 neonatal intensive care units throughout Japan and, from the responses, 13 patients who met the criteria (from 12 hospitals) were identified. HSV type 1 infection was detected in one patient (8%), and HSV type 2 infection in 5 patients (38%). Seven patients were tested by antibody or PCR examinations without specifying the subtypes. The ages at symptom onset ranged from 13 to 26 d of birth (mean: 17 d). The age at the last follow-up ranged from 2 to 76 months (30 months).

A structured research questionnaire was used to collect the following information regarding each identified patient: gestational age at birth, birth weight, age at onset and at the last follow-up visit, clinical signs and symptoms, maternal genital lesions present at the time of delivery, virological examinations, time course of neuroimaging, treatment, and outcome. The symptom onset was defined as the timing of initial manifestations including seizures, lethargy, poor feeding, fever, skin or mouth vesicles, conjunctivitis, keratitis, hepatopathy, coagulopathy and pneumonia. The ethics committee of Seirei-Hamamatsu General Hospital approved the study.

2.2. MRI studies

The following 4 time points from symptom onset were chosen for DWI and conventional MRI scans:

(1) Within 48 h of onset (≤48 h).
(2) During 3–7 d after onset (during 3–7 d).
(3) During 8–28 d after onset (during 8–28 d).

(4) At 29 d or later (only for conventional MRI; ⩾29 d).

Observed high-signal DWI abnormalities were classified as:

Type 1. Superficial cerebral lesions
- 1a. Cortical lesions: Only cortical lesions, not extending to the subcortical white matter (Fig. 1A and B).
- 1b. Cortical lesions + subcortical white matter lesions: Cortical lesions extending to the subcortical white matter lesions (Fig. 1C).

Type 2. Deep cerebral lesions including basal ganglia, internal capsule, and thalamus (Fig. 1D).

We analyzed a total of 32 DWI scans consisting of 9 scans in 7 patients <48 h, 11 scans in 9 patients during 3–7 d, and 12 scans in 10 patients during 8–28 d.

Apparent diffusion coefficient (ADC) maps were applied for 24 MRI scans in 10 patients. The low ADCs were available to confirm restricted diffusion in DWI (Fig. 1E and F). Unless ADC mapping was performed on the scans, we reviewed the possible effect of T2 shine though effects using T2-weighted and/or fluid-attenuated inversion recovery (FLAIR) images.

Conventional MRI scans were also collected, including T1-weighted, T2-weighted, and FLAIR images. We analyzed 9 scans for 7 patients ⩽48 h, 11 scans for 9 patients during 3–7 d, 12 scans for 10 patients during 8–28 d, and 11 scans for 10 patients ⩾29 d. We reviewed the abnormal signals in conventional MRI, including gray/white matter differentiation and hemorrhage, as well as atrophic and cystic changes. Conventional MRI data were compared to the changes observed using DWI.

We reviewed the location and size of the superficial cerebral lesions and the location of the deep cerebral lesion. We classified distributions of superficial cerebral lesions at ⩽7 d of onset into unilateral or bilateral lesions. We classified distributions of the deep cerebral lesions at ⩽7 d of onset into none, unilateral or bilateral lesions. DWI and conventional MRI scans were initially reviewed by one board certified pediatric neurologist (T. Okanishi). Thereafter, three other board certified pediatric neurologists (H. Yamamoto, J. Takanashi, A. Okumura) reviewed the images, and if necessary, they corrected the initial reports with their consensus. The three authors were unaware of the clinical information or scan time points of the patients.

Because this study was undertaken retrospectively at multiple institutions, the MRI protocols varied. The MRI field strength was 1.5 T for all scans. For each neonate, the acquisition parameters used with an FOV of 160–230 mm were as follows: DWI, TR = 2440–5200 ms and TE = 65–107 ms; T1-weighted imaging, TR = 442–3110 ms and TE = 10–15 ms; T2-weighted imaging, TR = 3800–43000 ms and TE = 85–115 ms; and FLAIR, TR = 9000–43000 ms, TE 95–102 ms, and TI = 200–2500 ms. The imaging matrix on DWI was 90–128 × 128. The slice thickness of DWI was 3–6 mm. The *b*-value was 0 and 1000, or 0 and 1200 s/mm^2.

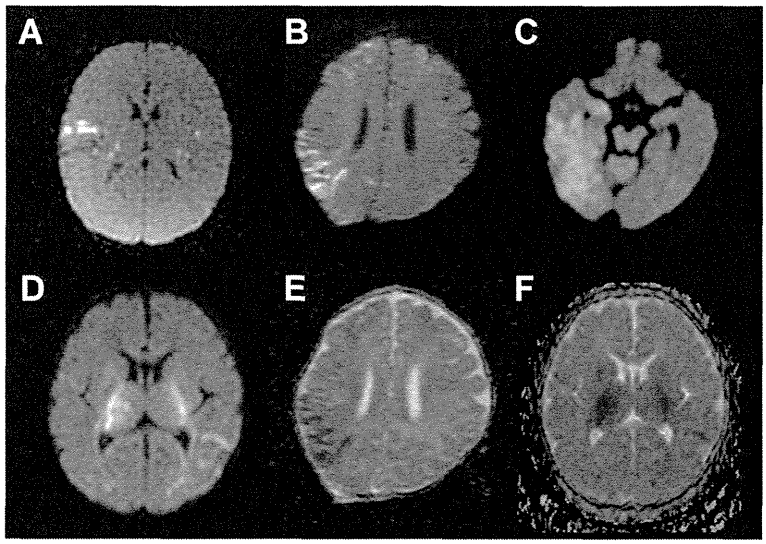

Fig. 1. Lesions on diffusion-weighted imaging. (A) (patient #4) and (B) (#5), cortical lesions; (C) (#12), cortical lesions + subcortical white matter lesions; (D) deep cerebral lesions (#10) in the internal capsules and thalamus. The distribution of high-signal lesions seen on (B) and (D) corresponded to the low diffusion area in apparent diffusion coefficient (ADC) maps ((E) and (F), respectively).

2.3. Clinical outcomes

Twelve patients were monitored for more than 6 months and we evaluated the motor and cognitive outcomes. Gross motor function was evaluated and described as: "normal," if milestone of the highest functions, including rolling (5 months old), sitting (7 months old), crawling (8 months old) and walking (12 months old), were >70% of those expected for the child's chronological age; "delayed," if the milestone behaviors were 31–70% of those expected for their chronological age; and as "severely delayed," if the milestones were <30% of those expected. Developmental quotient or intellectual quotient (DQ/IQ) score was evaluated, and described as follows: "normal," if >70% of the expected value for the child's chronological age; "delayed," if 31–70% of the expected value; and "severely delayed," if ⩽30% of the expected value. The DQ or IQ was measured using the Tsumori-Inage Developmental Assessment Test, Enjoji Analytical Development Test, Kyoto Scale of Psychological Development, and Tanaka-Binet Intelligence Scales according to the age of the patient and preference of each hospital.

2.4. Statistical analyses

We analyzed the correlation between the incidence of cortical lesions/cortical lesions + subcortical white matter lesions and the 3 time periods (⩽48 h, during 3–7 d, and 8–28 d). We analyzed the correlations of the distributions of the superficial cerebral lesions and the deep cerebral lesions at ⩽7 d of onset with the outcomes of gross motor function and DQ/IQ score. In patients with 2 or more DWI scans at ⩽7 d of onset, the most abnormal results were used. We analyzed the correlations of the timing of acyclovir therapy (⩽6 h, during 6–24 h, and over 24 h) with the outcomes. For these analyses, we used Spearman's rank correlation test. A value of $p < 0.05$ was considered significant. The statistical analyses were performed using Excel 2010 (Microsoft, Redmond, WA, USA) with a Statcel 3 add-in (OMS, Tokyo, Japan).

3. Results

3.1. Patient and clinical data

We present the clinical data in Supplementary Table. The records of 8 girls and 5 boys, born between October 2004 and June 2011, were reviewed. The patients had a mean gestational age of 40 weeks (range, 36–41 weeks) and a mean birth weight of 3216 g (2670–4196 g); and a mean age at symptom onset of 17 d (13–26 d).

The initial clinical symptoms included fever in 7 patients (54%), seizures in 5 (38%), lethargy in 3 (23%), and feeding impairment in 1 (8%). All patients presented with isolated encephalitis. Patient #3 presented with skin vesicles.

Throughout the acute clinical phase of the disease, 11 patients had experienced seizures by day 4. The remaining 2 patients had no seizure history. None of the patients demonstrated asphyxia, shock, cardiac arrest, or other serious complications.

HSV infection was confirmed by cerebrospinal fluid (CSF)-PCR in all patients, serum-PCR in 3 (14%), CSF-antibody in 2 (15%), serum-antibody in 4 (31%), and viral isolation from skin vesicles in 1 (8%). All the patients were treated with intravenous acyclovir (20–60 mg kg^{-1} day^{-1}).

3.2. Clinical outcomes

The ages range at the last follow-up ranged from 2 to 76 months (mean: 30 months). We excluded one patient (#2) after 2 months follow-up from the outcome evaluations. At the last follow-up assessment, motor function was "normal" in 6 patients (#3–5, 9, 11, and 13), "delayed" in 1 (#1), and "severely delayed" in 5 (#6–8, 10, and 12). DQ/IQ scores were "normal" in 3 patients (#4, 5 and 13), "delayed" in 5 (#1, 3, 8, 9, and 11), and "severely delayed" in 4 (#6, 7, 10, and 12).

The timing of acyclovir therapy did not show any significant correlations with motor functions ($p = 0.11$) or DQ/IQ scores ($p = 0.17$).

3.3. DWI studies

Table 1 describes DWI findings in each scan time point.

3.3.1. Superficial cerebral lesions

All scans obtained at ⩽7 d showed superficial cerebral lesions. Cortical lesions were evident on 8 scans (89%) of all 7 patients (#1–7) at ⩽48 h, 3 scans (27%) of 3 patients (#9, 11, and 13) during 3–7 d, and no scans during 8–28 d. Cortical lesions + subcortical white matter lesions were evident on 1 scan (11%, #1) at ⩽48 h, 8 scans (83%) of 6 patients (#3, 4, 7, 8, 10, and 12) during 3–7 d, of 9 scans (75%) on 9 patients (#1–4, 7, and 10–13) during 8–28 d. Multiple cortical lesions, ranging in size from <1 gyrus to ⩾3 gyri, were scattered throughout the cerebral cortices of both hemispheres of the patients. Within 48 h of onset, the lesions were distributed over 2–6 cerebral lobes The lesions were distributed unilaterally on 2 scans (22%) of 2 patients (#3 and 4) and bilaterally on 7 scans (78%) of 5 patients (#1, 2, and 5–7). During 3–7 d of onset, the lesions were distributed over 1–8 cerebral lobes. The lesions were distributed unilaterally of 2 scans (18%) in 2 patients (#9 and 11) and bilaterally on 9 scans (82%) of 7 patients (#3, 4, 7, 8, 10, 12, and 13). The lesions were asymmetrically distributed and not related to the arterial

Table 1
DWI findings within 7 d after onset.

Patient	≤ 48 hours of onset					3-7 d after onset				
	Hours	Types	Number of locations	Laterality	Locations	Days	Types	Number of locations	Laterality	Details
1	17	C	3	Bil.	R. F, T; L. F					
		D	3	Bil.	R. IC; Bil. Thalami				NA	
	40	C+WM	3	Bil.	R. F, T; L. F					
		D	3	Bil.	R. IC; Bil. Thalami					
2	19	C	2	Bil.	Bil. F				NA	
		D	1	Uni.	R. Thalamus					
3	20	C	2	Uni.	L. F, T	3	C+WM	3	Bil.	R. T; L. F, T
		D	1	Uni.	L. IC		D	1	Uni.	L. IC
4	23	C	2	Uni.	R. F, T	5	C+WM	3	Bil.	R. F, T; L. T
		D	2	Uni.	R. IC, Putamen		D	2	Uni.	R. IC, Putamen
5	26	C	6	Bil.	R. F, T, P, O; L. F, O				NA	
6	27	C	3	Bil.	R. F, T; L. F					
		D	4	Bil.	Bil. IC, Thalami				NA	
	42	C	3	Bil.	R. F, T; L. F					
		D	4	Bil.	Bil. IC, Thalami					
7	30	C	3	Bil.	R. F, T; L. T	6	C+WM	3	Bil.	R. F, T; L. T
		D	4	Bil.	Bil. IC, Thalami		D	4	Bil.	Bil. IC, Thalami
8	NA					3	C+WM	7	Bil.	R. F; Bil. T, P, O (MCA areas)
							D	4	Bil.	Bil. IC, Thalami
						5	C+WM	7	Bil.	R. F; Bil. T, P, O (MCA areas)
							D	2	Bil.	Bil. IC
9	NA					4	C	1	Uni.	L. T
10	NA					4	C+WM	6	Bil.	Bil. F, P, O (parasagittal)
							D	4	Bil.	Bil. IC, Thalami
						6	C+WM	8	Bil.	Bil. F, T, P, O (parasagittal)
							D	4	Bil.	Bil. IC, Thalami
11	NA					4	C	2	Uni.	R. F, T
12	NA					4	C+WM	5	Bil.	R. F, T, P, O; L. O
							D	4	Bil.	Bil. IC, Thalami
13	NA					5	C	3	Bil.	R. T; L. F, T

C, cortical lesions; C + WM, cortical + subcortical white matter lesions; D, deep cerebral lesions; R., right; L., left; Bil, bilateral; F, frontal lobe; T, temporal lobe; P, parietal lobe; O, occipital lobe; IC, internal capsule; NA, not available.

territories (Fig. 1A and B). In 7 patients, we confirmed consecutive changes of lesions extending from the cortex into the subcortical white matter (Fig. 2A and B). Such changes were found in 1 patient (#1) at ≤48 h, 3 patients (#3, 4, 7) ≤7 d, 1 patient (#2) at ≤28 d, and 2 patients (#11 and 13) during 3–28 d. The cortical lesions + subcortical white matter lesions were also distributed asymmetrically in most patients. Exceptional findings were observed in 2 patients and consisted of symmetrical, diffuse cortical and white matter lesions. The lesions were distributed in the regions of the posterior middle cerebral arteries on 2 scans (#8), and in the parasagittal area on 2 scans (#10). The signal intensities and the margins of the superficial cerebral lesions at ≤7 d became fainter and blurred during 8–28 d. Finally, the incidences of cortical or cortical + subcortical lesions were significantly correlated with the time point of DWI scans ($p < 0.01$).

Table 2 presents the distributions of DWI lesions at ≤7 d. Eleven patients (#1–8, 10, 12, and 13) showed bilateral superficial cerebral lesions. Two patients (#9 and 11) showed unilateral superficial cerebral lesions. Six patients (#2, 5, 6, 9, 11, and 13) showed cortical lesions at ≤7 d. Seven patients (#1, 3, 4, 7, 8, 10, and 12) showed cortical lesions + subcortical white matter lesions. The distributions of superficial cerebral lesions (unilateral or bilateral) did not correlate with outcomes of gross motor function or DQ/IQ scores.

3.3.2. Deep cerebral lesions

Deep cerebral lesions were found on 8 scans (89%) of 6 patients (#1–4, 6, and 7) at ≤48 h, in 8 scans (73%) of 6 patients (#3, 4, 7, 8, 10, and 12) during 3–7 d, and on 5 scans (45%) of 5 patients (#1, 2, 7, 10, and 12) during 8–28 d. All deep cerebral lesions coincided with the superficial cerebral lesions. Within 48 h of onset, the deep cerebral lesions distributed over 0–4 locations. The lesions were distributed unilaterally on 3 scans (33%) of 3 patients (#2–4) and bilaterally on 5 scans (56%) in 3 patients (#1, 6, and 7). During 3–7 d of onset, the deep cerebral lesions were distributed over 0–4 locations during 3–7 d. The lesions were distributed unilaterally on 2 scans (18%) of 2 patients (#3 and 4) and bilaterally on 6 scans (55%) of 4 patients (#7, 8, 10, and 12). The deep cerebral lesions in the internal capsules were found on 7 scans at ≤48 h, 8 scans during 3–7 d, and 5 scans during 8–28 d. Lesions in the thalamus were found on 6 scans at ≤48 h, 5 scans during 3–7 d, and in 5 scans during 8–28 d. Lesions in the putamen were found on 1 scan ≤48 h, 1 scan during 3–7 d, and were not found during 8–28 d.

Seven (#1, 2, 6–8, 10, and 12) patients showed bilateral deep cerebral lesions (Table 2). Two (#3 and 4) patients showed unilateral deep cerebral lesions. Four patients (#5, 9, 11, and 13) showed no deep cerebral lesions. All the patients with severely delayed outcomes of gross motor function and DQ/IQ scores displayed the bilateral deep cerebral lesions. The distributions of deep cerebral lesions (none, unilateral, bilateral) at ≤7 d were significantly correlated with poor outcomes of gross motor function ($p < 0.01$) and DQ/IQ scores ($p < 0.01$; Supplementary Figure). In this study, we found no patients with DWI lesions in either the brainstem or cerebellum.

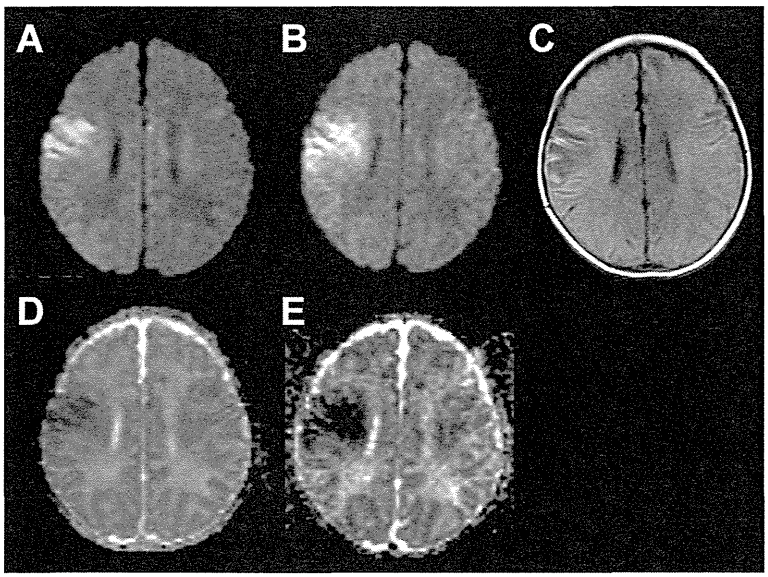

Fig. 2. Diffusion-weighted imaging (A and B) and T1-weighted imaging (C) in patient #1. (A) Cortical lesion in the right front temporal lobe, 17 h after onset; (B) extending to the subcortical white matter in the same area at 40 h after onset; (C) the lesion evolved into areas of encephalomalacia by day 14. The distribution of high-signal lesions on (A) and (B) corresponded to the low diffusion area in apparent diffusion coefficient maps (ADC) ((D) and (E), respectively).

Table 2
Distributions of diffusion-weighted imaging lesions within 7 d of onset relating with outcomes.

Patient	Cortical, subcortical white matter lesions		Deep lesions	Follow-up months	Gross motor function	DQ/IQ scores
	Bil./Uni.	C/C + WM	Bil./Uni./None			
1	Bil.	C + WM	Bil.	17	Delayed	Delayed
2	Bil.	C	Bil.	2	NA	NA
3	Bil.	C + WM	L.	76	Normal	Delayed
4	Bil.	C + WM	R.	43	Normal	Normal
5	Bil.	C	None	35	Normal	Normal
6	Bil.	C	Bil.	15	Severely delayed	Severely delayed
7	Bil.	C + WM	Bil.	13	Severely delayed	Severely delayed
8	Bil.	C + WM	Bil.	9	Severely delayed	Delayed
9	L.	C	None	60	Normal	Delayed
10	Bil.	C + WM	Bil.	25	Severely delayed	Severely delayed
11	R.	C	None	34	Normal	Delayed
12	Bil.	C + WM	Bil.	38	Severely delayed	Severely delayed
13	Bil.	C	None	26	Normal	Normal

Bil., bilateral; Uni., unilateral; R., right; L., left; C, cortical lesions; C + WM, cortical lesions + subcortical white matter lesions; DQ/IQ, developmental quotient or intellectual quotient; NA, not applicable.

3.3.3. ADC maps

Restricted diffusions upon DWI was confirmed on all 24 scans as low signals on ADC maps (Figs. 1E, F and 2D, E). The remaining 8 DWI images were analyzed for the presence of the T2 shine-through effect. Two scans of patient #12 showed high-signal regions on T2-weighted images corresponding to the DWI lesions. These lesions were small and did not affect the result of the analyses in this study.

3.3.4. Conventional MRI studies

T1- and T2-weighted images were obtained in all scans. FLAIR images were obtained in 27 scans.

Among the 20 total scans obtained at $\leqslant$7 d, conventional MRI scans showed signal changes in 11 patients: loss of gray/white matter differentiation (5 scans [25%]) and high-intensity signals in the cerebral cortex (10 scans [50%]), white matter (4 scans [20%]), or thalamus (1 study [5%]). These lesions were blurred or small compared to those observed on DWI. Conventional MRI did not detect any small (<1 gyrus) cortical lesions.

After 8 d of onset ($\geqslant$8 d), 23 total conventional MRI scans from 11 patients were analyzed. In all cases, the cortical lesions eventually evolved into encephalomalacia and/or atrophic changes (Fig. 2C). The thalamus and putamen lesions, visible on DWI in 9 patients at $\leqslant$7 d, changed to atrophy with high-intensity signals on T1-weighted or FLAIR images. Apart from 1 scan (#13, 14 d of onset), the lesions on conventional MRI were more distinct than those of DWI at $\geqslant$8 d.

Five patients (#2, 6, 7, 10, and 12) showed diffuse (>1 lobe) encephalomalacia with atrophic changes in both hemispheres at $\geqslant$8 d. MRI showed focal (<3 gyri) encephalomalacia in 1 hemisphere in 1 patient (#4) and both hemispheres in 5 patients (#1, 3, 8, 11, and 13). One patient (#1) demonstrated growing cysts in the left hemisphere at 3 months of age.

We did not find lesions in any of the patients at any time point in either the cerebellum or brainstem.

4. Discussion

As the time from symptom onset increased, the cortical lesions extended to subcortical white matter. The lesion progressions strongly indicate herpes encephalitis in newborns. Deep cerebral DWI lesions at $\leqslant$7 d of symptom onset in NHSE are prognostic factors for neurological outcomes.

The cortical lesions were characteristically evident as multiple, scattered lesions, asymmetrically distributed and not related to the major arterial territories. This cortical lesion pattern was previously reported in three cases with the scan time points of 20 h to 5 d from onsets [12,14,15]. Our study revealed that DWI is the most sensitive brain imaging technique available to reveal cortical lesion patterns in the early period ($\leqslant$48 h) of the onset of NHSE.

The early DWI patterns of NHSE are different from those of ischemia and other central nervous system infections. The DWI patterns of thrombotic brain infarction involved the cerebral cortex and correlated with the territories of the large- or medium-sized arteries, with the lesions being distinct in the white matter rather than in the cortices [17–19]. Neonatal bacterial brain infections show DWI patterns typical of watershed or major arterial infarctions, or brain abscesses in the white matter [15,20]. In 2 cases with parechovirus or coxsackie B2 virus, MRI showed symmetrical lesions in both cortices and white matter [21,22]. Depending on their size and distribution, the scattered and asymmetrical cortical lesions can suggest an NHSE diagnosis. Because virological examinations regularly yield false-negative results and the results that are also slow to obtain [6], brain DWI can facilitate a rapid

and early diagnosis of NHSE. Although early acyclovir therapy did not show any correlation with the neurological outcomes in this study, the presence of the cortical lesions on brain DWI can strongly indicate starting or continuing acyclovir therapy in neonates.

HSV has a high affinity for neurons and may initially infect the cortical neurons of NHSE patients [23]. In adult HSE, HSV initially disseminates to one or both mesial temporal lobes by retrograde transmission via the olfactory nerves [24]. The multiple and scattered cortical abnormalities in DWI that appear to be associated with NHSE are specific to newborns. Gutierrez et al. hypothesized that in infants with isolated HSE, maternally derived transplacental neutralizing antibodies in the infants' serum prevent hematogenous transmission; thus, the retrograde transmission causes isolated encephalitis [25]. The multiple scattered neocortical lesions observed at $\leqslant$7 d in the present study suggest that hematogenous transmission is the main route of infection in NHSE.

Kubota et al. previously reported the progression of lesions from cerebral cortex to subcortical white matter in 1 (#3) of the current patients [14]. We confirmed this phenomenon in 6 additional patients (#1, 2, 4, 7, 11, and 13) within 4 weeks of symptom onset. HSV shows a specific cell-to-cell infection pattern via nectin binding on cell surface [23]. This form of transmission may account for the phenomenon of lesions spreading from the cortex to the subcortical white matter.

The bilateral deep cerebral lesions at $\leqslant$7 d correlated with poor neurological outcomes. The patients with severely delayed development showed extended encephalomalacia in the cerebrums. In newborns with hypoxic-ischemic encephalopathy, DWI lesions in bilateral posterior limb of the internal capsule predict poor neurological outcomes [16]. Here, 5 of 6 patients with NHSE had bilateral deep cerebral lesions including the internal capsule lesions in our cases. Similar to hypoxic–ischemic encephalopathy, the damaged posterior limb of the internal capsules by NHSE might precipitate poor neurological outcomes.

This study has some limitations. The imaging techniques varied in each hospital, and these differences might have affected the sensitivity of DWI. It is difficult to differentiate between the cortex and white matter in neonates has difficulties. Therefore the selected cortical lesions are more likely to be located in the superficial cortex. In 2 data, the high-signal DWI lesions might actually be T2 shine through effect. The time point of DWI scans depended on each physician's decision. Although there was one case report of cerebellar and brainstem lesion [13] and fatal cases of disseminated herpes infection [11], we had no such cases in this study. Early and consecutive changes in DWI of neonatal brain infections other than HSV also have not been sufficiently documented. Thus, DWI investigations of other infections are necessary to evaluate the specificity of the changes we found in the present study.

Financial disclosure

There are no financial relationships relevant to this manuscript to disclose.

Acknowledgments

The authors are grateful to Drs. Motoo Nakagawa, MD, Ph.D., and Kenji Yokochi, MD, Ph.D., for advice regarding the MRI findings; to Ayako Ochi, MD, for advice regarding study design; and to Drs. Shin-ichiro Hamano, MD, Ph.D.; Takashi Ichiyama, MD, Ph.D.; Akira Sasaki, MD; Makoto Kuwashima, MD; Kaori Irahara, MD, for assembling the patient data.

Appendix A. Supplementary data

Supplementary data associated with this article can be found, in the online version, at http://dx.doi.org/10.1016/j.braindev.2014.07.006.

References

[1] Brown RS. Herpes simplex virus encephalitis in the newborn. Dev Med Child Neurol 1977;19:407–10.
[2] Kimberlin D. Herpes simplex virus, meningitis and encephalitis in neonates. Herpes 2004;11(Suppl. 2):65A–76A.
[3] Whitley R. Neonatal herpes simplex virus infection. Curr Opin Infect Dis 2004;17:243–6.
[4] Kimberlin DW, Lin CY, Jacobs RF, Powell DA, Frenkel LM, Gruber WC, et al. Natural history of neonatal herpes simplex virus infections in the acyclovir era. Pediatrics 2001;108:223–9.
[5] Whitley R, Arvin A, Prober C, Corey L, Burchett S, Plotkin S, et al. Predictors of morbidity and mortality in neonates with herpes simplex virus infections. The National Institute of Allergy and Infectious Diseases Collaborative Antiviral Study Group. N Engl J Med 1991;324:450–4.
[6] Malm G, Forsgren M. Neonatal herpes simplex virus infections: HSV DNA in cerebrospinal fluid and serum. Arch Dis Child Fetal Neonatal Ed 1999;81:F24–9.
[7] Kirkham FJ. Guidelines for the management of encephalitis in children. Dev Med Child Neurol 2013;55:107–10.
[8] Enzmann D, Chang Y, Augustyn G. MR findings in neonatal herpes simplex encephalitis type II. J Comput Assist Tomogr 1990;14:453–7.
[9] Breningstall GN, Patterson RJ. Convalescence disguising disease progression in neonatal herpes encephalitis. Pediatr Neurol 2010;42:298–300.
[10] Toth C, Harder S, Yager J. Neonatal herpes encephalitis: a case series and review of clinical presentation. Can J Neurol Sci 2003;30:36–40.
[11] Vossough A, Zimmerman RA, Bilaniuk LT, Schwartz EM. Imaging findings of neonatal herpes simplex virus type 2 encephalitis. Neuroradiology 2008;50:355–66.
[12] Dhawan A, Kecskes Z, Jyoti R, Kent AL. Early diffusion-weighted magnetic resonance imaging findings in neonatal herpes encephalitis. J Paediatr Child Health 2006;42:824–6.

[13] Pelligra G, Lynch N, Miller SP, Sargent MA, Osiovich H. Brainstem involvement in neonatal herpes simplex virus type 2 encephalitis. Pediatrics 2007;120:e442–6.
[14] Kubota T, Ito M, Maruyama K, Kato Y, Miyajima Y, Ogawa A, et al. Serial diffusion-weighted imaging of neonatal herpes encephalitis: a case report. Brain Dev 2007;29:171–3.
[15] Teixeira J, Zimmerman RA, Haselgrove JC, Bilaniuk LT, Hunter JV. Diffusion imaging in pediatric central nervous system infections. Neuroradiology 2001;43:1031–9.
[16] Goergen SK, Ang H, Wong F, Carse EA, Charlton M, Evans R, et al. Early MRI in term infants with perinatal hypoxic–ischaemic brain injury: interobserver agreement and MRI predictors of outcome at 2 years. Clin Radiol 2014;69:72–81.
[17] Rutherford MA, Ramenghi LA, Cowan FM. Neonatal stroke. Arch Dis Child Fetal Neonatal Ed 2012;97:F377–84.
[18] Wraige E, Pohl KR, Ganesan V. A proposed classification for subtypes of arterial ischaemic stroke in children. Dev Med Child Neurol 2005;47:252–6.
[19] Dudink J, Mercuri E, Al-Nakib L, Govaert P, Counsell SJ, Rutherford MA, et al. Evolution of unilateral perinatal arterial ischemic stroke on conventional and diffusion-weighted MR imaging. AJNR Am J Neuroradiol 2009;30:998–1004.
[20] Jan W, Zimmerman RA, Bilaniuk LT, Hunter JV, Simon EM, Haselgrove J. Diffusion-weighted imaging in acute bacterial meningitis in infancy. Neuroradiology 2003;45:634–9.
[21] Verboon-Maciolek MA, Groenendaal F, Hahn CD, Hellmann J, van Loon AM, Boivin G, et al. Human parechovirus causes encephalitis with white matter injury in neonates. Ann Neurol 2008;64:266–73.
[22] Hirata O, Ishikawa N, Mizoguchi Y, Nakamura K, Kobayashi M. A case of neonatal coxsackie B2 meningo-encephalitis in which serial magnetic resonance imaging findings reveal the development of lesions. Neuropediatrics 2011;42:156–8.
[23] Spear PG. Herpes simplex virus: receptors and ligands for cell entry. Cell Microbiol 2004;6:401–10.
[24] Steiner I. Herpes simplex virus encephalitis: new infection or reactivation? Curr Opin Neurol 2011;24:268–74.
[25] Gutierrez KM, Whitley RJ, Arvin AM. Herpes simplex virus infections. In: Remington JS, Klein JO, Wilson CB, Nizet V, Maldonado Y, editors. Infectious diseases of the fetus and newborn infant. Philadelphia: Saunders; 2011. p. 813–33.

European Journal of Medical Genetics 58 (2015) 369–371

Contents lists available at ScienceDirect

European Journal of Medical Genetics

journal homepage: http://www.elsevier.com/locate/ejmg

Clinical report

Progressive brain atrophy in Schinzel–Giedion syndrome with a *SETBP1* mutation

Akihito Takeuchi [a, *], Nobuhiko Okamoto [b], Shoko Fujinaga [c], Hirosuke Morita [a], Junya Shimizu [c], Tomoyuki Akiyama [d], Shinsuke Ninomiya [e], Jun-ichi Takanashi [f], Toshihide Kubo [c]

[a] *Department of Neonatology, Okayama Medical Center, National Hospital Organization, Okayama, Japan*
[b] *Department of Medical Genetics, Osaka Medical Center and Research Institute for Maternal and Child Health, Osaka, Japan*
[c] *Department of Pediatrics, Okayama Medical Center, National Hospital Organization, Okayama, Japan*
[d] *Department of Child Neurology, Okayama University Hospital, Okayama, Japan*
[e] *Department of Medical Genetics, Kurashiki Central Hospital, Kurashiki, Japan*
[f] *Department of Pediatrics, Tokyo Women's Medical University Yachiyo Medical Center, Yachiyo, Japan*

ARTICLE INFO

Article history:
Received 20 February 2015
Accepted 31 May 2015
Available online 19 June 2015

Keywords:
Schinzel-Giedion syndrome
SETBP1
Brain atrophy
Magnetic resonance imaging
Diffusion weighted imaging

ABSTRACT

Schinzel-Giedion syndrome is a rare congenital malformation syndrome. Recently, *SETBP1* was identified as the causative gene. Herein, we present a Japanese boy with Schinzel-Giedion syndrome resulting from a novel mutation in *SETBP1* in order to establish the clinical features and serial MRI findings associated with the syndrome. On the third day of life, the boy was referred to our hospital because of facial abnormalities and feeding difficulty. Midfacial retraction, frontal bossing, deep groove under the eyes, upturned nose, low-set ears, bilateral cryptorchidism, and generalized hypertrichosis were identified on admission. At the age of 7 months, epileptic spasms in series occurred. Based on characteristic facial and skeletal abnormalities and severe developmental delay, we clinically diagnosed him with Schinzel-Giedion syndrome. Direct sequencing of the *SETBP1* gene revealed a heterozygous mutation (p.Ile871Ser) in exon 4. Although neither cardiac defect nor choanal stenosis were present in our case, the phenotype of our case was nearly identical to those of previously reported cases confirmed by genetic analysis. Serial MRI from the age of 1 month–3 years revealed progressive brain atrophy, especially in the white matter and basal ganglia. However, myelination was age-appropriate and no obvious abnormal signals in the white matter were seen. Diffusion weighted imaging revealed no abnormal findings. Accumulation of MRI data including diffusion weighted imaging from Schinzel-Giedion syndrome cases is needed to understand the mechanism underlying progressive brain atrophy in this syndrome.

1. Introduction

Schinzel-Giedion syndrome (SGS) (MIM #269150) is a rare congenital malformation syndrome characterized by midfacial retraction, frontal bossing, deep grooves under the eyes, severe mental retardation, epilepsy, and multiple anomalies such as heart defects, hydronephrosis, hypertrichosis, and radiographic skeletal anomalies (Schinzel and Giedion, 1978). Almost half of all patients with SGS die within the first two years of life due to various causes such as epilepsy, respiratory failure, and infection (Jones, 2013). Moreover, an increased prevalence of neuroepithelial tumors has been reported in SGS (Lehman et al., 2008). Recently, Hoischen et al. have revealed that heterozygous de novo mutations in the SET binding protein 1 (*SETBP1*) gene are the genetic cause of SGS (Hoischen et al., 2010). To date, seven different mutations in *SETBP1* have been reported in 18 patients with SGS (Hoischen et al., 2010; Ko et al., 2013; Suphapeetiporn et al., 2011; Carvalho et al., 2015; Lopez-Gonzalez et al., 2015). Herein, we present a Japanese boy with SGS resulting from a novel mutation in *SETBP1* and report his serial magnetic resonance imaging (MRI) findings including diffusion-weighted imaging (DWI).

* Corresponding author. Department of Neonatology, Okayama Medical Center, National Hospital Organization, 1711-1 Tamasu, Kita-ku, Okayama, 701-1192, Japan.
E-mail address: gmd18025@s.okayama-u.ac.jp (A. Takeuchi).

http://dx.doi.org/10.1016/j.ejmg.2015.05.006
1769-7212/

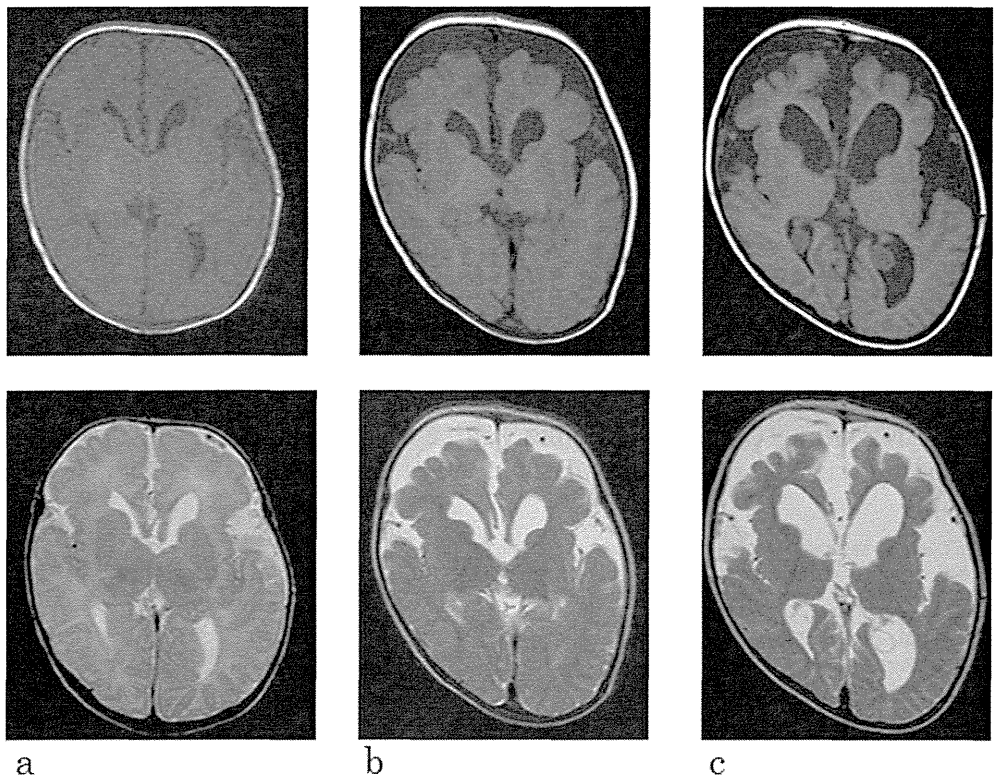

Fig. 1. Serial Conventional MRIs. T1 weighted images are shown in the upper row and T2 weighted images in the lower row in chronological order. Only mild dilatation of the lateral ventricles was seen at the age of 1 month (a). Marked progressive brain atrophy was evident at the age of 1 year 3 months (b) and at the age of 3 years 3 months (c).

2. Clinical report

A boy was referred to our hospital on his third day of life because of facial abnormalities and feeding difficulty. He was born as the first baby from non-consanguineous Japanese parents after an uneventful full-term gestation. His birth weight was 3,388 g (+0.5SD), birth height was 46.7 cm (−1.8SD), and head circumference was 32.3 cm (−1.1SD). The Apgar score was 9 at 1 min and 10 at 5 min. His parents had no significant past medical history or family history. Facial dysmorphism was noted at birth, and feeding difficulty became evident within two days after birth. He was admitted to the neonatal intensive care unit in our hospital.

Midfacial retraction, frontal bossing, deep groove under the eyes, upturned nose, low-set ears, bilateral cryptorchidism, and generalized hypertrichosis were identified on admission. Ultrasonography revealed no congenital heart defect or hydronephrosis. X-rays of extremities and trunk revealed widening of distal femurs and broad ribs. Brain MRI at 1 month of age showed only mild enlargement of the lateral ventricles. The auditory brainstem response threshold was elevated (right side 60 dB nHL, left side 80 dB nHL). No significant abnormality was detected by means of blood tests including complete blood cell count, blood gas analysis, conventional biochemical test, thyroid function test, amino acid analysis, and lysosomal enzyme activity analysis. The results of urinary organic acid and uronic acid analyses were also normal. A G-band chromosomal analysis revealed a 46, XY karyotype.

After his admission, the proportion of oral feeding was gradually increased until he could be fed orally with an adequate amount of mother's milk. He was discharged from our hospital without a

Table 1
Clinical features of SGS cases with *SETBP1* mutations.

Mutation sites[a]	Present case	Reported cases						
	p.I871S	p.I871T (n = 5)	pS867R (n = 1)	p.D868N (n = 5)	p.D868A (n = 1)	p.G870D (n = 1)	p.G870S (n = 4)	p.G870C (n = 1)
Gender[b]	M	M3· F2	F	M3· F2	F	M	M3· F1	M
Neurodevelopmental delay	+	4/4	1/1	5/5	1/1	1/1	4/4	1/1
Seizure	+	4/5	1/1	5/5	1/1	1/1	4/4	1/1
Vision impairment	unknown	3/4	1/1	3/3	1/1	unknown	1/3	unknown
Hearing impairment	+	4/4	unknown	3/3	0/1	unknown	3/3	unknown
Typical craniofacial features	+	5/5	1/1	5/5	1/1	1/1	4/4	1/1
Genital anomaly	+	5/5	1/1	5/5	1/1	1/1	4/4	unknown
Hydronephrosis or VUR	+	5/5	0/1	5/5	1/1	1/1	4/4	1/1
Cardiac defect	−	2/5	0/1	3/4	1/1	0/1	1/3	0/1
Skeletal malformations	+	4/4	0/1	3/3	1/1	1/1	4/4	1/1
Choanal stenosis	−	2/5	unknown	2/4	0/1	0/1	0/4	unknown

[a] I: Isoleucine, S: Serine, T: Threonine, R: Arginine, D: Aspartic acid, N: Asparagine, A: Alanine, G: Glycine, C: Cysteine.
[b] M: Male, F: Female.

nasogastric tube at the age of 1 month. An electroencephalogram (EEG) at 1 month of age revealed a few multifocal epileptiform discharges. At the age of 7 months, his EEG showed typical hypsarrhythmia and epileptic spasms in series occurred. His development before the onset of infantile spasms was severely delayed; he could not control his head and did not engage in visual tracking. Based on his characteristic facial and skeletal abnormalities and developmental delay, we clinically diagnosed him with SGS (Lehman et al., 2008). Direct sequencing of his *SETBP1* gene revealed a novel heterozygous mutation (p.Ile871Ser) in exon 4. This mutation was de novo.

For treatment of his infantile spasms, considering the limited effect of ACTH therapy for patients with SGS (Grosso et al., 2003), we chose anti-epileptic drug therapy. He required tube feeding after the onset of infantile spasms because his feeding difficulty worsened. Gastrostomy was performed at the age of 2 years 1 month. Ultrasonography and abdominal MRI revealed bilateral hydronephrosis. He is now 3 years 3 months old. He is bedridden and cannot track objects with his eyes, control his head, or speak meaningful words. His epileptic spasms have not been suppressed by anti-epileptic drugs. Screening for tumors is performed every 6 months by abdominal ultrasonography, thoracic-abdominal MRI and blood test including alpha feto-protein (AFP) and human chorionic gonadotropin beta subunit, but no tumor development has been detected to date.

Brain MRI was performed at the age of 1 month and again at 1 year 3 months, 2 years, 2 years 4 months, and 3 years 3 months. In addition to conventional MR images, we obtained DWI at 2 years 4 months and at 3 years 3 months (Fig. 1). Although the patient's MRI showed only mild dilatation of the lateral ventricles at the age of 1 month (Fig. 1a), follow-up MRI showed progressive brain atrophy involving the white matter, basal ganglia, thalamus, brainstem, and cerebellum (Fig. 1b, c). Myelination of his brain has developed to an appropriate degree for his age, and no obvious abnormal signals in the white matter have been seen in MRI to date (Fig. 1a–c). No abnormalities of apparent diffusion coefficient (ADC) values in the white matter were detected in DWI at the age of 2 years or at 2 years 4 months. Additionally, Periventricular heterotopia at right anterior horn was revealed by conventional MRIs.

3. Discussion

Clinical features of the current patient and previously reported SGS cases with *SETBP1* mutations are shown in Table 1 (Hoischen et al., 2010; Ko et al., 2013; Suphapeetiporn et al., 2011; Carvalho et al., 2015; Lopez-Gonzalez et al., 2015). Although in the present case hydronephrosis was not detected during the neonatal period, it did become obvious after the age of 2 years. The phenotype of our case is nearly identical to those of previously reported cases.

We found a novel mutation of *SETBP1* in the present case (p.Ile871Cys). To date, seven other mutations of *SETBP1* (p.Ser867Arg, p.Asp868Asn, p.Asp868Ala, p.Gly870Asp, p.Gly870Ser, p.Gly870Cys, p.Ile871Thr) have been reported in patients with SGS (Hoischen et al., 2010). The sites of these mutations, including that in the present case (P.Ile871Cys), are concentrated in four sequences of five consecutive amino acids each on the SETBP1 protein (Ser867, Asp868, Gly870, Ile871).

In the present case, progressive marked brain atrophy was seen in serial MRIs. However, no apparent abnormalities were detected with regard to either myelination or the ADC value in white matter. Little is known about the mechanism of progressive brain atrophy in patients with SGS. Pathological examination of the brain of an SGS patient who presented with progressive dilatation of the lateral ventricles on serial ultrasonography and died nine weeks after birth due to prolonged apnea revealed gliosis in the subependymal layer and no histological evidence of an infective or inflammatory process (Maclennan et al., 1991). Previous study have shown progressive brain atrophy in other patients with SGS (Shah et al., 1999). Considering that clinical features of the current patient were identical to those of previously reported cases with other *SETBP1* mutations, progressive brain atrophy was thought to be not specific for *SETBP1* p.I871S mutation but a common SGS feature that was just underdiagnosed.

In one report of a case clinically diagnosed as SGS, MRI showed delayed myelination and decreased ADC values in the occipital and temporal white matter, but it should be noted that the facial characteristics in this case were different from those of typical SGS, and genetic diagnosis was not performed (Watanabe et al., 2012).

Accumulation of serial MRI data including DWI from SGS cases is necessary to understand the mechanism underlying brain atrophy in SGS.

Acknowledgments

We appreciate the valuable comments provided by Dr. Misao Kageyama, Dr. Makoto Nakamura, Dr. Kazue Nakamura, Dr. Yuko Yumoto, Dr. Shigehiro Mori, Dr. Kei Tamai, Dr. Kyohei Takahashi, Dr. Hiroki Tsuchiya and Dr. Yuki Hyodo. The authors have no conflicts of interest to disclose.

References

Carvalho, E., Honjo, R., Magalhaes, M., Yamamoto, G., Rocha, K., Naslavsky, M., et al., 2015. Schinzel-Giedion syndrome in two Brazilian patients: report of novel mutation in SETBP1 and literature review of the clinical features. Am. J. Med. Genet. A 167, 1039–1046.

Grosso, S., Pagano, C., Cioni, M., Di Bartolo, R.M., Morgese, G., Balestri, P., 2003. Schinzel–Giedion syndrome: a further cause of West syndrome. Brain Dev. 25, 294–298. http://dx.doi.org/10.1016/s0387-7604(02)00232-2.

Hoischen, A., van Bon, B.W.M., Gilissen, C., Arts, P., van Lier, B., Steehouwer, M., et al., 2010. De novo mutations of SETBP1 cause Schinzel-Giedion syndrome. Nat. Genet. 42, 483–485. http://dx.doi.org/10.1038/ng.581.

Jones, Kenneth Lyons, 2013. Smith's Recognizable Patterns of Human Malformation, seventh ed. Elsevier Saunders, Philadelphia, pp. 302–303.

Ko, J.M., Lim, B.C., Kim, K.J., Hwang, Y.S., Ryu, H.W., Lee, J.H., et al., 2013. Distinct neurological features in a patient with Schinzel-Giedion syndrome caused by a recurrent SETBP1 mutation. Childs Nerv. Syst. 29, 525–529. http://dx.doi.org/10.1007/s00381-013-2047-2.

Lehman, A.M., McFadden, D., Pugash, D., Sangha, K., Gibson, W.T., Patel, M.S., 2008. Schinzel-Giedion syndrome: report of splenopancreatic fusion and proposed diagnostic criteria. Am. J. Med. Genet. A 146A, 1299–1306. http://dx.doi.org/10.1002/ajmg.a.32277.

Lopez-Gonzalez, V., Domingo-Jimenez, M.R., Burglen, L., Ballesta-Martinez, M.J., Whalen, S., Pinero-Fernandez, J.A., et al., 2015. Schinzel-Giedion syndrome: a new mutation in SETBP1. An Pediatr (Barc) 82, e12–e16 (in Spanish).

Maclennan, A.C., Doyle, D., Simpson, R.M., 1991. Neurosonography and pathology in the Schinzel-Giedion syndrome. J. Med. Genet. 28, 547–549. http://dx.doi.org/10.1136/jmg.28.8.547.

Schinzel, A., Giedion, A., 1978. A syndrome of severe midface retraction, multiple skull anomalies, clubfeet, and cardiac and renal malformations in sibs. Am. J. Med. Genet. 1, 361–375. http://dx.doi.org/10.1002/ajmg.1320010402.

Shah, A.M., Smith, M.F., Griffiths, P.D., Quarrell, O.W.J., 1999. Schinzel-Giedion syndrome: evidence for a neurodegenerative process. Am. J. Med. Genet. 82, 344–347. http://dx.doi.org/10.1002/(SICI)1096-8628(19990212)82, 4 <344::AID-AJMG13>3.0.CO;2-H.

Suphapeetiporn, K., Srichomthong, C., Shotelersuk, V., 2011. SETBP1 mutations in two Thai patients with Schinzel-Giedion syndrome. Clin. Genet. 79, 391–393. http://dx.doi.org/10.1111/j.1399-0004.2010.01552.x.

Watanabe, S., Murayama, A., Haginoya, K., Tanaka, S., Togashi, N., Abukawa, D., et al., 2012. Schinzel-Giedion syndrome: a further cause of early myoclonic encephalopathy and vacuolating myelinopathy. Brain Dev. 34, 151–155. http://dx.doi.org/10.1016/j.braindev.2011.03.010.

CLINICAL GENETICS An International Journal of Genetics, Molecular and Personalized Medicine

Clin Genet 2015: 87: 395–397
Printed in Singapore. All rights reserved

CLINICAL GENETICS
doi: 10.1111/cge.12455

Letter to the Editor

Atypical giant axonal neuropathy arising from a homozygous mutation by uniparental isodisomy

To the Editor:

Gigaxonin, encoded by *GAN*, is essential for neuronal survival and mutations in *GAN* cause autosomal recessive giant axonal neuropathy 1 (GAN1, MIM 256850), which affects both the central and peripheral nervous systems (1, 2).

Uniparental disomy (UPD) is defined as inheritance of a pair of chromosomes or segments from only one parent, while duplication of a single parental allele is designated as uniparental isodisomy (UPiD) (3). UPiD harboring a homozygous mutation can be a genetic cause of autosomal recessive disorders. Here, we present a clinically undiagnosed patient with GAN1 caused by segmental maternal UPiD with a homozygous splice-site mutation in *GAN*, which is readily detected by whole-exome sequencing (WES).

An 18-year-old female was the first child of non-consanguineous parents. Her mother had mild intellectual disability. Her initial motor development was normal until frequent falls at 4 years of age. At age 6, low body height (101.2 cm, −3 SD), weight (13.4 kg, −2.3 SD), and frizzy hair were noted (Fig. 1a). Brain magnetic resonance imaging (MRI) and nerve conduction studies identified leukoencephalopathy and sensory-motor neuropathy, respectively. Scoliosis appeared at age 7. Her educational achievement at school started to decline at age 8. Sural nerve biopsy at age 10 revealed marked loss of large myelinated fibers (Fig. S1a,b, Supporting Information). Psychomotor regression gradually progressed. At age 13, she lost ambulation. Brain MRI showed a cystic lesion in the cerebellar white matter with right-side predominance. At age 15, non-invasive positive pressure ventilation was introduced for her restrictive respiratory failure due to progressive scoliosis. At present, nystagmus, facial muscle weakness, dysarthria, mild dysphagia, distal dominant muscle atrophy and weakness, absent deep tendon reflexes, negative Babinski sign, disturbances in superficial/deep sensation, and ataxia are observed. She is currently bed-bound, with mild intellectual disability and progressive sensory-motor neuropathy (Table 1). Brain MRI T2-weighted images show diffuse high signal intensities in the cerebral/cerebellar white matter, basal ganglia, and thalamus, but sparing the U-fibers and the corpus callosum. The cystic lesion in the cerebellar white matter has progressed (Figs. 1b,c and S1c,d).

Table 1. Nerve conduction studies of the patient[a]

		DL (m s)	Amp	Velocity (m/s)
At age 13 years				
R median N	MCS	5.55	2.79 mV	39.6
	SCS	–	Not evoked	–
R ulnar N	MCS	3.65	4.21 mV	41.3
	SCS	4.4	1.5 uV	18.2
R tibial N	MCS	–	Not evoked	–
R peroneal N	MCS	–	Not evoked	–
R sural N	SCS	–	Not evoked	–
At age 18 years				
R median N	MCS	4.2	0.732 mV	41.4
R ulnar N	MCS	5.8	0.743 mV	36.2

Amp, amplitude at wrist; DL, distal latency; MCS, motor conduction study; N, nerve; R, right; SCS, sensory conduction study.
[a]Only action potentials of median and ulnar nerves were evoked. Compound muscle action potentials (CMAPs) and sensory nerve action potentials (SNAPs) in median and ulnar nerves were severely reduced compared to the mild reduction in the motor/sensory nerve conduction velocity. Distal latencies were mildly prolonged. The reduction in CMAP progressed over time.

After obtaining the informed consent, WES was performed in a proband and her parents, identifying a novel homozygous splice-site mutation (c.1237-1G>A) in *GAN*, which was validated by Sanger sequencing (Fig. 1d). Reverse transcription polymerase chain reaction (RT-PCR) identified skipping of *GAN* exon 8, leading to a frame-shift (p.Ile413ValfsX22) (Fig. 1e). Interestingly, only the mother had the mutation as heterozygote. Using WES data, homozygosity mapping and copy number analysis found loss of heterozygosity at 16q23.1-qter (chr16:78790765-89944842) (including *GAN*) and two copies of this interval, respectively, suggesting UPiD (Figs. 1f and S1e). Two copies of *GAN* were confirmed by quantitative real-time PCR (Fig. S1f). WES genotyping suggested maternal isodisomy at 16q23.2-qter leading to unmasking of a recessive splice-site mutation in *GAN* (Fig. 1g). Methods are detailed in Appendix S1.

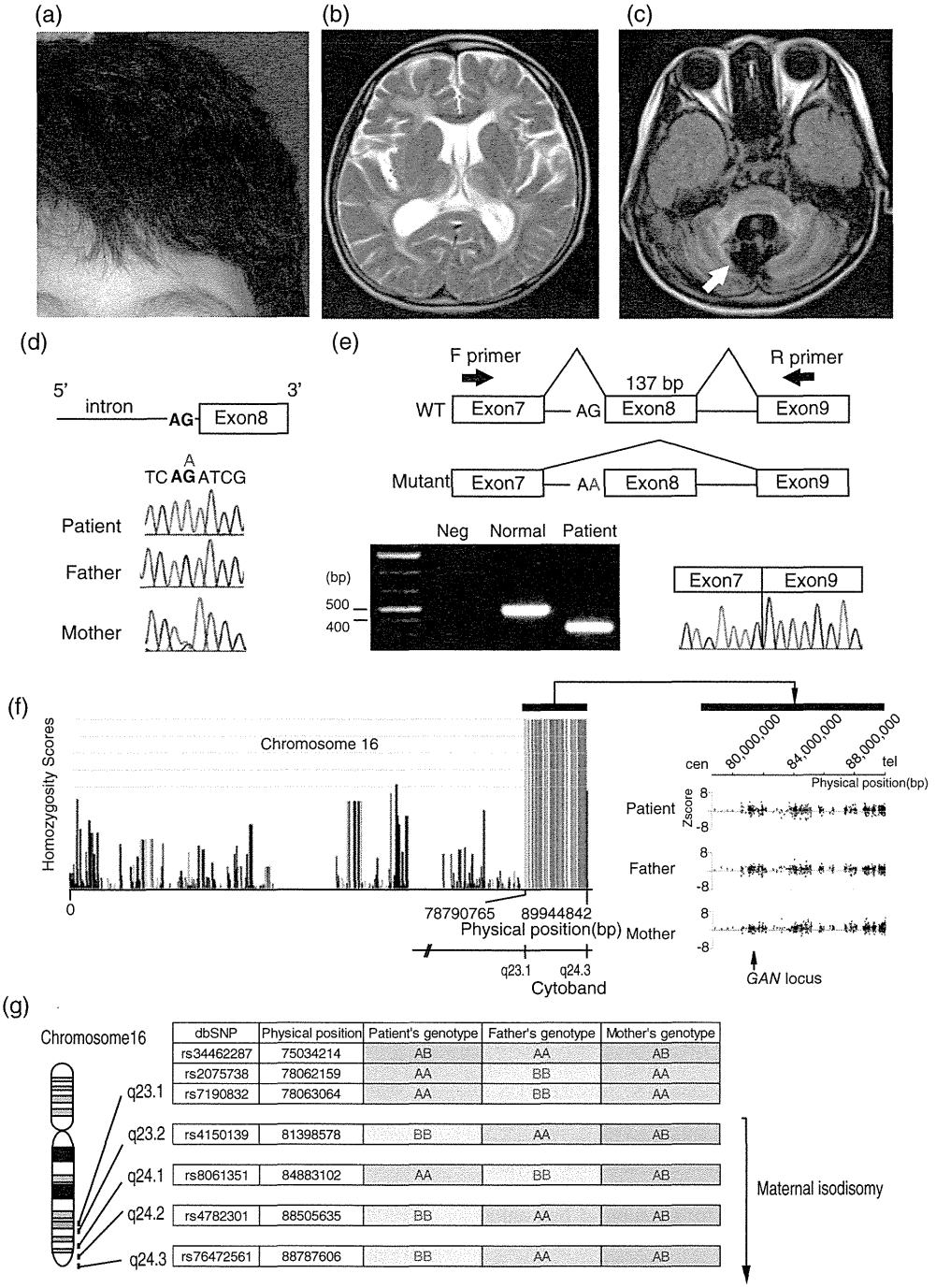

dbSNP	Physical position	Patient's genotype	Father's genotype	Mother's genotype
rs34462287	75034214	AB	AA	AB
rs2075738	78062159	AA	BB	AA
rs7190832	78063064	AA	BB	AA
rs4150139	81398578	BB	AA	AB
rs8061351	84883102	AA	BB	AB
rs4782301	88505635	BB	AA	AB
rs76472561	88787606	BB	AA	AB

Fig. 1. Clinical and genetic analyses of the patient with GAN1 (**a**) frizzy hair of the patient. (**b**, **c**) Brain MRI of the GAN1 patient at 18 years of age. Axial T2-weighted images (**b**) demonstrate diffuse signal abnormalities in cerebral white matter, sparing the corpus callosum and U-fibers. The posterior limb of the internal capsule and thalamus also shows high signal intensities. Axial FLAIR images (**c**) demonstrate high signal intensities in the cerebellar white matter, pyramidal tract, and medial lemniscus of the brain stem. The cystic lesion in the cerebellar hemisphere, with right-side predominance (involving the dentate nucleus hilus) was progressively observed from 13 years of age (arrow). (**d**) Sanger sequencing of the *GAN* mutation (c.1237-1G>A). The mutation was located within a canonical acceptor site of exon 8. Note that the father is wild-type, the mother heterozygote, and the patient homozygote. (**e**) The c.1237-1G>A mutation causes skipping of exon 8 in *GAN*. A reverse transcription polymerase chain reaction (RT-PCR) product spanning exons 7–9 was 137-bp shorter in the patient than a normal control. Sanger sequencing of the RT-PCR product from the patient confirmed exon 8 skipping. (**f**) Left panel: Homozygosity mapping of whole-exome sequencing (WES) data on chromosome 16 using HomozygosityMapper. *x*-axis shows the physical position on chromosome 16 and *y*-axis shows homozygosity scores. The interval indicated by red bars (chr16:78790765-89944842) is the homozygous region. Right panel: Enlarged view of copy number analysis of WES data from the homozygous region using eXome Hidden Markov Model (XHMM). *x*-axis shows the physical position on chromosome 16. *y*-axis shows *Z* scores for the depth of coverage at each locus. There were no copy number changes in this region among the trio (patient, father, and mother). (**g**) Genotyping analysis of WES data surrounding the *GAN* locus from the patient and her parents revealed maternal isodisomy at 16q23.2-qter in the patient.

The diagnostic utility of WES has been increasingly reported for patients with suspected genetic disorders (4). As in this case, WES may identify genetic causes for cases with a broader phenotypic spectrum. The cystic lesion we identified by MRI has not been previously reported in GAN1. T2-weighted images of GAN1 demonstrate variable cerebral/cerebellar white matter abnormalities with pathological astrocytic gliosis, variable myelin loss, and scattered Rosenthal fibers (2, 5). Interestingly cystic degeneration can emerge in later stages of Alexander's disease (6), with brain MRI findings and Rosenthal fiber deposition resembling those of GAN1 (2)

Segmental UPiD16 observed here is possibly explained by non-disjunction during meiosis I, preceded by recombination at 16q23.2-qter and following loss of paternal chromosome 16 (trisomy rescue) (Fig. S2), as previously described (7). Intrauterine growth retardation or congenital anomalies that may be associated with UPD16 (7) was not observed.

In conclusion, WES data are useful for copy number, loss of heterozygosity, and mutational analyses, and will enable genetic diagnoses of clinically undiagnosed cases.

Supporting Information

Additional supporting information may be found in the online version of this article at the publisher's web-site.

Acknowledgements

We thank all the participants for their cooperation in this research. We also thank Dr K. Nishiyama, Ms K. Takabe, Mr T. Miyama, Ms A. Narita, Ms N. Watanabe, Ms S. Sasamoto, and Ms S. Sugimoto, from the Department of Human Genetics, Yokohama City University Graduate School of Medicine, for their technical assistance. This work was supported by the Ministry of Health, Labour and Welfare of Japan (J. T., N. Miyake, N. Matsumoto); the Japan Society for the Promotion of Science (a Grant-in-Aid for Scientific Research (C) (26461549) (S. M.), a Grant-in-Aid for Scientific Research (B) (25293085, 25293235) (N. Miyake, H. S.), a Grant-in-Aid for Scientific Research (A) (13313587) (N. Matsumoto), and a Grant-in-Aid for Challenging Exploratory Research (26670505) (H. S.); the Takeda Science Foundation (N. Miyake, H. S., N. Matsumoto); the Yokohama Foundation for Advancement of Medical Science (S. M.); the Fund for Creation of Innovation Centers for Advanced Interdisciplinary Research Areas Program in the Project for Developing Innovation Systems (N. Matsumoto); the Strategic Research Program for Brain Sciences (11105137) (N. Matsumoto); and a Grant-in-Aid for Scientific Research on Innovative Areas (Transcription Cycle) from the Ministry of Education, Culture, Sports, Science and Technology of Japan (12024421) (N. Miyake, N. Matsumoto).

S. Miyatake[a]
H. Tada[b]
S. Moriya[a]
J. Takanashi[c]
Y. Hirano[d]
M. Hayashi[e]
Y. Oya[f]
M. Nakashima[a]
Y. Tsurusaki[a]
N. Miyake[a]
N. Matsumoto[a]
H. Saitsu[a]
[a]Department of Human Genetics, Yokohama City University Graduate School of Medicine, Yokohama, Japan,
[b]Department of Pediatrics, Chibaken Saiseikai Narashino Hospital, Narashino, Japan,
[c]Department of Pediatrics, Tokyo Women's Medical University, Yachiyo Medical Center, Yachiyo-shi, Japan,
[d]Department of Pediatrics, Tokyo Women's Medical University, Tokyo, Japan,
[e]Department of Brain Development and Neural Regeneration, Tokyo Metropolitan Institute of Medical Science, Tokyo, Japan,
[f]Department of Neurology, National Center Hospital, National Center of Neurology and Psychiatry, Tokyo, Japan

References

1. Bomont P, Cavalier L, Blondeau F et al. The gene encoding gigaxonin, a new member of the cytoskeletal BTB/kelch repeat family, is mutated in giant axonal neuropathy. Nat Genet 2000: 26: 370–374.
2. van der Knaap M, Valk J. Magnetic resonance of myelination and myelin disorders. Heidelberg, Germany: Springer, 2005.
3. Engel E. A new genetic concept: uniparental disomy and its potential effect, isodisomy. Am J Med Genet 1980: 6: 137–143.
4. Yang Y, Muzny DM, Reid JG et al. Clinical whole-exome sequencing for the diagnosis of Mendelian disorders. N Engl J Med 2013: 369: 1502–1511.
5. Kretzschmar HA, Berg BO, Davis RL. Giant axonal neuropathy. A neuropathological study. Acta Neuropathol 1987: 73: 138–144.
6. van der Knaap MS, Naidu S, Breiter SN et al. Alexander disease: diagnosis with MR imaging. AJNR Am J Neuroradiol 2001: 22: 541–552.
7. Catarzi S, Giunti L, Papadia F et al. Morquio A syndrome due to maternal uniparental isodisomy of the telomeric end of chromosome 16. Mol Genet Metab 2012: 105: 438–442.

Correspondence:
Satoko Miyatake, MD, PhD
Department of Human Genetics
Yokohama City University Graduate School of Medicine
3-9 Fukuura, Kanazawa-ku
Yokohama 236-0004
Japan
Tel.: +81 45 7872606
Fax: +81 45 7865219
e-mail: miyatake@yokohama-cu.ac.jp

ELSEVIER

Brain & Development 38 (2016) 142–144

BRAIN & DEVELOPMENT
Official Journal of the Japanese Society of Child Neurology

www.elsevier.com/locate/braindev

Case Report

White matter abnormalities in an adult patient with L-2-hydroxyglutaric aciduria

Toshiyuki Yamamoto [a,*], Seiichiro Yoshioka [b], Yoshinori Tsurusaki [c], Shimada Shino [a,d], Keiko Shimojima [a], Yosuke Shigematsu [e], Yoshihiro Takeuchi [b], Naomichi Matsumoto [c]

[a] *Tokyo Women's Medical University Institute for Integrated Medical Sciences, Tokyo, Japan*
[b] *Department of Pediatrics, Shiga Medical University, Ohtsu, Japan*
[c] *Department of Human Genetics, Yokohama City University Graduate School of Medicine, Yokohama, Japan*
[d] *Department of Pediatrics, Tokyo Women's Medical University, Tokyo, Japan*
[e] *Department of Health Science, Faculty of Medical Sciences, University of Fukui, Japan*

Received 7 April 2015; received in revised form 30 April 2015; accepted 30 April 2015

Abstract

L-2-Hydroxyglutaric aciduria (L-2-HGA) is a rare inborn error of metabolism. Mainly, patients with this disorder exhibit neurological symptoms and characteristic neuroradiological findings, such as subcortical white matter abnormalities, which are believed to be caused by the toxicity of the accumulation of L-2-hydroxyglutaric acid. A genotype-first approach of the whole exome sequence was used to identify compound heterozygous mutations, c.584A>G (p.Y195C) and c.772T>C (p.C258R), in *L2HGDH*, the gene responsible for this disorder, in an adult patient with intellectual disability and intractable epilepsy. A retrospective assay confirmed the increased concentrations of 2-hydroxyglutaric acid in the urine. These results suggested that neuroradiological findings of subcortical white matter abnormalities are characteristic of L-2-HGA and that clinical exome sequencing has sufficient power to compensate for insufficient clinical evaluations.

Keywords: L-2-Hydroxyglutaric aciduria (L-2-HGA); *L2HGDH*; Subcortical white matter abnormalities; Genotype-first approach; Clinical exome sequencing

1. Introduction

L-2-Hydroxyglutaric aciduria (L-2-HGA; MIM#236792) is a rare inborn error of metabolism, which involves defects in the metabolism of L-2-hydroxyglutaric acid, which results in increased levels of the acid in the urine. Since the first case was described in 1980 [1], some cases have been reported in Japan [2] and worldwide. The gene responsible for this disorder, *L2HGDH*, which is located on chromosome 14q22.1, was identified in 2004 [1]. The pathogenesis of the accumulation of L-2-hydroxyglutaric acid is unclear, but it is probably toxic to the white matter through myelin vacuolation [3]. Consequently, the neuroradiological findings in these patients are unique, and the subcortical white matter abnormalities can be visualized with brain magnetic resonance imaging (MRI) [4].

Although the diagnosis of an inborn error of metabolism can generally be made by screening of the metabolic

* Corresponding author at: Tokyo Women's Medical University Institute for Integrated Medical Sciences, 8-1 Kawada-cho, Shinjuku-ward, Tokyo 162-8666, Japan. Tel.: +81 3 3353 8112x24013; fax: +81 3 5269 7667.
E-mail address: yamamoto.toshiyuki@twmu.ac.jp (T. Yamamoto).

http://dx.doi.org/10.1016/j.braindev.2015.04.012
0387-7604/

substrate, such an error is often undiagnosed because of phenotypic heterogeneity. Recent advancements in molecular analysis equipment have overcome this dilemma in clinical diagnosis. Some cases with inborn error of metabolism have been diagnosed with genotype-first approach and not by metabolism screening [5,6]. Here, we present a new patient with L-2-HGA who exhibited white matter abnormalities and who was diagnosed by clinical exome sequencing.

2. Patient report

A 33-year-old female patient was born with a birth weight of 2500 g (mean), a length of 47.5 cm (25th–50th centile), and an occipitofrontal circumference (OFC) of 32 cm (10th–20th centile). Her parents were non-consanguineous and healthy. She has four siblings. She started to show recurrent febrile seizures at 7 months. She began to walk with supports at 10 months and to talk with meaningful words at 9 months. Her neurodevelopment was within normal limits until 8 years of age. At that time, she exhibited nonfebrile seizures. Because an electroencephalography showed right-frontal dominant spike and wave discharges, anti-epileptic drugs were prescribed. Subsequently, her psychomotor development gradually delayed. Her generalized tonic seizures were intractable, and several attacks were observed per year. Because her intellectual capacity is at the approximate level of a 5-year-old, she lives in a group home that is supported by welfare.

At 33 years of age, she suddenly showed status epilepticus that was associated with drowsiness and without any trigger. She was immediately transferred to the hospital. Although she recovered consciousness after treatment, a brain MRI revealed abnormal findings in the white matter for the first time (Fig. 1).

At present, her height is 164 cm (90th–97th centile), her weight is 85 kg (>97th centile), and her OFC is 54 cm (10th centile), which indicates that she is obese with a body mass index of 31.6. A physical examination showed no abnormalities. A neurological examination revealed mild ataxia and dystonic posture. After obtaining the molecular diagnosis, combined D-2- and L-2-hydroxyglutaric acid levels in urine were measured using urease-pretreatment of urine, trimethylsilylation, and gas chromatography-mass spectrometry [7]. Although an increased concentration was detected, D-2- and L-2-hydroxyglutaric acids cannot be separated in this method.

3. Molecular analysis

The ethical committee of Tokyo Women's Medical University approved this study. After obtaining written informed consent from the patient's family, blood samples were obtained from the patient and her parents. DNA was extracted from the blood samples using QIAamp DNA extraction kit (QIAGEN GmbH, Hilden, Germany). DNA from the patient and her parents were analyzed with whole exome sequencing as previously described [8].

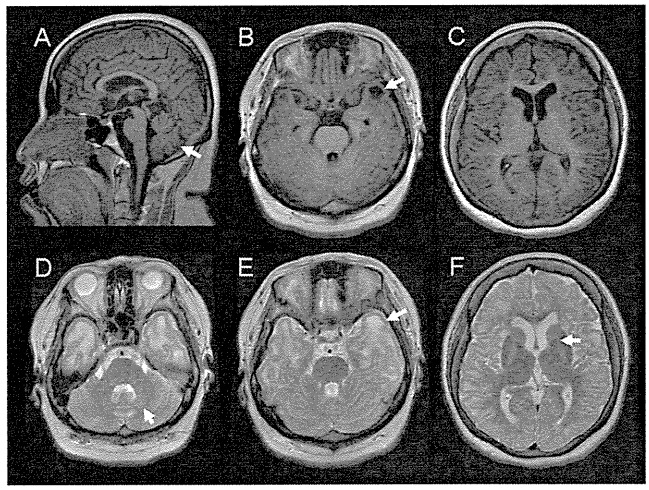

Fig. 1. The results of the brain magnetic resonance imaging that was performed on the patient at 33 years of age. (A) A T1-weighted sagittal image shows remarkable folia of the cerebrum (arrow), indicating mild atrophy. (B and C) T1-weighted axial images. (D–F) T2-weighted axial images. Diffuse subcortical white matter abnormalities are noted in axial images. Some of the subcortical regions (arrows) show cystic changes (B and D). The involvement of the dentate nucleus (arrow) is characteristic (D). Signal high intensity is shown in the anterior and posterior limbs of internal capsule (F). Dilatations of the lateral ventricles and extra-cerebral spaces indicate diffuse brain atrophy.

We focused on *de novo* and recessive mutations. Although there were no *de novo* mutations that have functional relevance to neurological disorders, we identified the following compound heterozygous mutations of *L2HGDH*: c.584A>G (p.Y195C) and c.772T>C (p.C258R). These mutations were transmitted from her father and mother, respectively. Sanger sequencing confirmed these findings (Fig. 2). The c.772T>C mutation is registered in the dbSNP137 SNP database as rs145390085, and it has a frequency of 0.007% in the National Heart, Lung, and Blood Institute Exome Sequencing Project (NHLBI-ESP) 6500 (http://evs.gs.washington.edu/EVS/). The c.584A>G mutation is not registered in the dsSNP137 SNP database, NHLBI-ESP 6500, Human Genetic Variation Browser database (http://www.genome.med.kyoto-u.ac.jp/SnpDB/), or in any of our 575 in-house Japanese control exome databases. The c.584A>G and c.772T>C mutations were predicted to be damaging by SIFT (http://sift.jcvi.org/) scores of 0.00 for both, Polyphen-2 (http://genetics.bwh.harvard.edu/pph2/) scores of 0.986 and 1.000, respectively, and MutationTaster (http://neurocore.charite.de/MutationTaster/) scores of 1.000 for both.

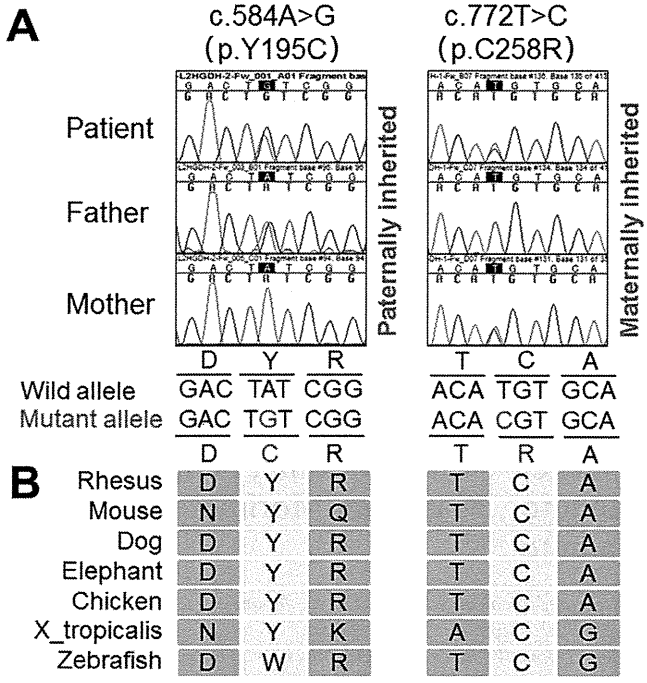

Fig. 2. The results of the molecular analysis. (A) Sanger sequencing confirms compound heterozygous mutations that are transmitted from both parents. (B) The affected amino acids are conserved among mammals.

4. Discussion

In this study, we identified compound heterozygous variants of *L2HGDH* in an adult patient with epilepsy and intellectual disability. The paternally transmitted c.584A>G mutation was previously reported as a disease-causing mutation by Sass et al. [9]. In comparison, the maternally transmitted c.772T>C mutation was registered in the dbSNP database. However, its frequency was extremely low (0.007%), and the prediction software suggested that the consequence of this variant would be damaging. Therefore, we concluded that this variant was pathogenic. Urine screening that was performed after identification of the *L2HGDH* mutations detected an increased concentration of 2-hydroxyglutaric acid in the urine, and a final diagnosis of L-2-HGA was made in this patient.

Although this patient did not show developmental delay in early infancy, she started to show epilepsy and subsequent developmental deterioration at 8 years of age. This clinical course is typical for patients with L-2-HGA [10], but it is not specific and is also rather frequently observed in the histories of patients with intractable epilepsy. From the characteristic white matter abnormalities that were revealed by MRI, which the patient first underwent at 33 years of age after her status epilepticus, we suspected leukoencephalopathy, and we performed genetic screening. Although a diagnosis of L-2-HGA is generally made after findings of highly increased levels of L-2-hydroxyglutaric acid in the urine, a urine screening was never performed in this patient before the exome sequencing results were obtained. Therefore, a brain MRI examination and urine screening should have been performed in the early stages of the disease in this patient. Furthermore, a candidate diagnosis of L-2-HGA might have possibly been obtained after careful evaluation of the characteristic MRI findings [4]. Because there is a report of therapeutic approach using riboflavin, early diagnosis of L-2-HGA would be required [1].

Acknowledgements

We would like to express our gratitude to the patient and her parents for their cooperation. This work was supported by a Grant-in-Aid for Scientific Research from Health Labor Sciences Research Grants from the Ministry of Health, Labor, and Welfare, Japan.

References

[1] Kranendijk M, Struys EA, Salomons GS, Van der Knaap MS, Jakobs C. Progress in understanding 2-hydroxyglutaric acidurias. J Inherit Metab Dis 2012;35:571–87.
[2] Fujitake J, Ishikawa Y, Fujii H, Nishimura K, Hayakawa K, Inoue F, et al. L-2-Hydroxyglutaric aciduria: two Japanese adult cases in one family. J Neurol 1999;246:378–82.
[3] van der Knaap MS, Jakobs C, Hoffmann GF, Nyhan WL, Renier WO, Smeitink JA, et al. D-2-Hydroxyglutaric aciduria: biochemical marker or clinical disease entity? Ann Neurol 1999;45:111–9.
[4] Steenweg ME, Salomons GS, Yapici Z, Uziel G, Scalais E, Zafeiriou DI, et al. L-2-Hydroxyglutaric aciduria: pattern of MR imaging abnormalities in 56 patients. Radiology 2009;251:856–65.
[5] Prada CE, Gonzaga-Jauregui C, Tannenbaum R, Penney S, Lupski JR, Hopkin RJ, et al. Clinical utility of whole-exome sequencing in rare diseases: galactosialidosis. Eur J Med Genet 2014;57:339–44.
[6] Schuster J, Khan TN, Tariq M, Shaiq PA, Mabert K, Baig SM, et al. Exome sequencing circumvents missing clinical data and identifies a BSCL2 mutation in congenital lipodystrophy. BMC Med Genet 2014;15:71.
[7] Kuhara T. Diagnosis and monitoring of inborn errors of metabolism using urease-pretreatment of urine, isotope dilution, and gas chromatography-mass spectrometry. J Chromatogr B Analyt Technol Biomed Life Sci 2002;781:497–517.
[8] Tsurusaki Y, Koshimizu E, Ohashi H, Phadke S, Kou I, Shiina M, et al. De novo SOX11 mutations cause Coffin–Siris syndrome. Nat Commun 2014;5:4011.
[9] Sass JO, Jobard F, Topcu M, Mahfoud A, Werle E, Cure S, et al. L-2-Hydroxyglutaric aciduria: identification of ten novel mutations in the L2HGDH gene. J Inherit Metab Dis 2008;31(Suppl.):S275–9.
[10] Steenweg ME, Jakobs C, Errami A, van Dooren SJ, Adeva Bartolome MT, Aerssens P, et al. An overview of L-2-hydroxyglutarate dehydrogenase gene (L2HGDH) variants: a genotype-phenotype study. Hum Mutat 2010;31:380–90.

ELSEVIER

Brain & Development 37 (2015) 960–966

BRAIN & DEVELOPMENT
Official Journal of the Japanese Society of Child Neurology

www.elsevier.com/locate/braindev

Original article

Mutations in the genes encoding eukaryotic translation initiation factor 2B in Japanese patients with vanishing white matter disease

Shino Shimada [a,b], Keiko Shimojima [a], Noriko Sangu [a,c], Ai Hoshino [d], Yasuo Hachiya [d], Tatsuyuki Ohto [e], Yuichiro Hashi [f], Katsuya Nishida [g], Maki Mitani [g], Saori Kinjo [h], Yoshinori Tsurusaki [i], Naomichi Matsumoto [i], Masafumi Morimoto [j], Toshiyuki Yamamoto [a,*]

[a] *Tokyo Women's Medical University Institute for Integrated Medical Sciences, Tokyo, Japan*
[b] *Department of Pediatrics, Tokyo Women's Medical University, Tokyo, Japan*
[c] *Department of Oral and Maxillofacial Surgery, School of Medicine, Tokyo Women's Medical University, Tokyo, Japan*
[d] *Department of Neuropediatrics, Tokyo Metropolitan Neurological Hospital, Fuchu, Japan*
[e] *Department of Pediatrics, Tsukuba University, Tsukuba, Japan*
[f] *Department of Neurology, National Hospital Organization Kyoto Medical Center, Kyoto, Japan*
[g] *Department of Neurology, National Hospital Organization Hyogo-Chuo National Hospital, Sanda, Japan*
[h] *Department of Pediatrics, Okinawa Chubu Hospital, Uruma, Japan*
[i] *Department of Human Genetics, Yokohama City University Graduate School of Medicine, Yokohama, Japan*
[j] *Department of Pediatrics, Kyoto Prefectural University of Medicine, Kyoto, Japan*

Received 29 September 2014; received in revised form 4 March 2015; accepted 19 March 2015

Abstract

Objective: Vanishing white matter disease (VWM) is a chronic, progressive leukoencephalopathy associated with episodes of rapid deterioration following minor stress events such as head traumas or infectious disorders. The white matter of the patients with VWM exhibits characteristic radiological findings.

Method: The genes encoding all five subunits of eukaryotic translation initiation factor 2B (EIF2B) were analyzed in patients, who were tentatively diagnosed with VWM, by Sanger sequencing.

Results: Seven mutations were identified in the genes encoding the subunits 1, 2, 4, and 5 of EIF2B. Among them, one mutation (p.V83E) in the subunit 2 (*EIF2B2*) was recurrently identified in three alleles, indicating the most common mutation in Japanese patients with VWM. Two patients were homozygous, and the other four patients were compound heterozygous.

Conclusion: All patients showed white matter abnormalities with various degrees. One patient showed manifestations of end-stage VWM disease. Some patients showed late onset and slow progression associated with brain magnetic resonance imaging displaying T2 high intensity only in the deep white matter. There was clinical heterogeneity among patients with VWM.

Keywords: Vanishing white matter disease (VWM); Eukaryotic translation initiation factor 2B (EIF2B); Leukoencephalopathy; Mutation

* Corresponding author at: Tokyo Women's Medical University Institute for Integrated Medical Sciences, 8-1 Kawada-cho, Shinjuku-ward, Tokyo 162-8666, Japan. Tel.: +81 3 3353 8112x24013; fax: +81 3 5269 7667.
E-mail address: yamamoto.toshiyuki@twmu.ac.jp (T. Yamamoto).

http://dx.doi.org/10.1016/j.braindev.2015.03.003
0387-7604/

1. Introduction

Childhood ataxia with central hypomyelination (CACH) or leukoencephalopathy with vanishing white matter (VWM; MIM #603896) is a chronic, progressive leukoencephalopathy associated with episodes of rapid deterioration following minor stress events such as head trauma or infectious disorders [1–3]. Patients with VWM show abnormal radiological findings in the brain; i.e., the cerebral white matter appears progressively diffuse and symmetrical abnormalities such as rarefaction and cysts. VWM is an autosomal recessive disease caused by mutations in any of the genes encoding the subunits of eukaryotic translation initiation factor 2B (EIF2B), which is a GTP exchange protein essential for protein synthesis [4,5]. Until now, many disease-causing mutations have been identified [6–16].

In this study, we report on the results of our on-going study to obtain genetic diagnosis for Japanese patients with VWM.

2. Materials and methods

2.1. Patients and samples

This study was approved by the ethics committee at the Tokyo Women's Medical University. After obtaining written informed consents from patients or their families, blood samples were obtained from patients. Patients were recruited under candidate diagnosis of VWM as defined by previously proposed diagnostic criteria by van der Knaap et al. [17]. In the early stages of VWM, white matter involvements may not fulfill the criteria. Therefore, patients who did not show full manifestations but were tentatively diagnosed as VWM were also included in this study. Genomic DNAs were extracted from blood samples using the QIAamp DNA Mini Kit (QIAGEN, Hamburg, Germany). Parental samples were also obtained to confirm inheritance patterns.

2.2. Molecular analysis

All exons of the genes encoding the five subunits of EIF2B (*EIF2B1*, *EIF2B2*, *EIF2B3*, *EIF2B4*, and *EIF2B5*) were genotyped using standard Sanger sequencing. Information on the primers used for this study can be obtained upon request. When heterozygous or homozygous variations were identified in patients, inherited patterns were analyzed using corresponding parental samples. PCR products were subcloned into the pGEM® T-vector (Promega, Madison, WI) to identify the allelic locations of the mutation as described previously [18]. Subsequently, nucleotide sequences of inserted fragments were analyzed in both directions. When a *de novo* mutation was suspected, the biological relationship between the patient and the corresponding parental samples was confirmed by microsatellite marker analysis using the Linkage Mapping Set (Life Technologies, Foster City, CA) as described previously [19].

The identified non-synonymous variants were tested for mutational effects using damaging predication scores obtained from the SIFT [20] (http://sift.jcvi.org/), PolyPhen-2 [21] (http://genetics.bwh.harvard.edu/pph2/), and Combined Annotation-Dependent Depletion (CADD) [22] (http://cadd.gs.washington.edu/info) in accordance with methods reported elsewhere [23]. Interspecies amino acids conservation was checked using the UCSC Genome Bioinformatics Site (https://genome.ucsc.edu/).

3. Results

3.1. Pathogenic mutations

We analyzed a total of 22 patients. Among them, we identified mutations in the genes encoding the EIF2B subunits in six patients including four unrelated individuals and two siblings. All identified mutations were missense mutations (Supplemental Figs. 1 and 2). The results of the molecular analyses in accordance with the clinical information of the patients are summarized in Table 1. Patients 1 and 2 showed homozygous mutations in *EIF2B1* and *EIF2B2*, respectively. Patient 2 was homozygous for p.V83E in *EIF2B2*, and patient 3 had compound heterozygous mutations associated with p.V83E in *EIF2B2*. The other patients showed compound heterozygous mutations in either of *EIF2B2*, *EIF2B4* and *EIF2B5*. Parental origins of all mutations other than p.M305I were confirmed (Table 1). Predicted scores for the deleterious effects of mutations provided by SIFT, Polyphen-2, and CADD are included in Table 1.

Both p.M305I and p.I385T were identified in exon 7 of *EIF2B5* in patient 6. To assess the allelic locations of these two mutations, PCR products were subcloned into the plasmid vector. At least 10 clones were isolated and sequenced. Consequently, all clones showed one of the mutations, indicating that the two mutations were located on the independent alleles. Although p.I385T was identified in the patient's mother, p.M305I was not identified in both parents. We confirmed the biological relationship between patient 6 and his parents by linkage analysis (data not shown).

3.2. Patient reports

Patient 1 is a 61-year-old female, whose parents were cousins. Initial neurological symptoms with gait disturbance were first observed at 29 years of age. At that time, her intellectual quotient was evaluated to be 66. Motor incoordination and spasticity were also noted. Routine laboratory examinations of blood, urine, and

Table 1
Summaries of the clinical information of the patients and the results of mutation analyses.

Patients	Patient 1	Patient 2	Patient 3		Patient 4		Patient 5		Patient 6	
Clinical information										
Gender	F	F	M		M		M		M	
Present age (y/m)	61y	8y	8 m		22y		19y		5y5m	
Onset age (y/m)	29y	3y	8 m		13y		13y		13m	
Provoking event	–	Infection	Infection (fever)		Lack of sleep		Head trauma		Infection (fever)	
Seizure	+	+	+		+		–		+	
Disturbed consciousness	+	+	+		–		+		+	
Other neurological findings	Bedridden	Bulbar paralysis	Spasticity, developmental delay		Mild ataxia		Muscular weakness		Gait disturbance	
Consanguinity	+	–	–		–		–		–	
Family history	–	–	–		The elder brother of Pt. 5		The younger brother of Pt. 4		–	
Identified mutations										
Genes	*EIF2B1*	*EIF2B2*	*EIF2B2*		*EIF2B4*		*EIF2B4*		*EIF2B5*	
Chromosomal location	12q24.31	14q24.3	14q24.3		2p23.3		2p23.3		3q27.1	
Inheritance	Homozygous	Homozygous	Compound heterozygous		Compound heterozygous		Compound heterozygous		Compound heterozygous	
Exon	exon 8	exon 2	exon 2	exon 5	exon 6	exon 11	exon 6	exon 11	exon 7	exon 7
Nucleotide alteration	c.715T>G	c.254T>A	c.254T>A	c.682A>G	c.556T>A	c.1070G>A	c.556T>A	c.1070G>A	c.915G>A	c.1154T>C
Amino-acid change	p.F239V	p.V85E	p.V85E	p.R228G	p.Y186N	p.R357Q	p.Y186N	p.R357Q	p.M305I	p.I385T
Novel/ recurrent	Novel	Recurrent	Recurrent	Novel	Novel	Recurrent	Novel	Recurrent	Novel	Novel
Origin	Not confirmed	Both parents	Paternal	Maternal	Maternal	Paternal	Maternal	Paternal	*de novo*	Maternal
dbSNP build 138	–	–	–	–	–	rs113994033	–	rs113994033	–	–
Damaging prediction										
SIFT score	0.12	0.00	0.00	0.00	0.25	0.15	0.25	0.15	0.13	0.00
SIFT prediction	T	D	D	D	T	T	T	T	T	D
Polyphen2 HVAR score	0.715	0.995	0.995	0.999	0.979	0.637	0.979	0.637	0.196	0.95
Polyphen2 HVAR prediction	P	D	D	D	D	P	D	P	B	D
CADD score (raw)	5.436	5.264	5.264	3.760	4.290	5.227	4.290	5.227	3.735	4.732
CADD score (PHRED-like)	35.0	33.0	33.0	19.1	22.4	33.0	22.4	33.0	19.0	26.4

F, female; M, male; y, years; m, months; Pt., Patient; HVAR, HumVar-trained model autosomal recessive pattern; T, tolerate; D, damaging; B, benign.

cerebrospinal fluid (CSF) showed normal results. Enzyme activities including arylsulfatase A, β-hexosaminidase A, β-mannosidase, and α-fucosidase were within the normal limits. The motor nerve conduction velocity of the left peroneal nerve was 32 m/s, which indicated a delay. Cranial computed tomography showed diffusely distributed low-absorption in the white matter (no more detailed information). Her neurological deterioration progressed, and she is now bedridden. Brain magnetic resonance imaging (MRI) performed at 60 years of age showed diffuse high intensity in the T2-weighted images (Fig. 1).

Patient 2 is an 8-year-old girl. Language developmental delay was noted at 3 years of age. At 7 years, she was admitted to the hospital due to drowsiness after an infectious disease of mycoplasma pneumonia. Due to frequent seizures and respiratory failure, intubation was performed. Brain MRI showed diffuse T2 high